Amorphization and Fracture in Silicon Diselenide Nanowires: A Molecular Dynamics Study

Wei Li, Rajiv K. Kalia, and Priya Vashishta

Concurrent Computing Laboratory for Materials Simulations, Department of Physics and Astronomy, Department of Computer Science, Louisiana State University, Baton Rouge, Louisiana 70803-4001

(Received 4 April 1996)

Dynamics of amorphization and fracture in $SiSe_2$ nanowires are studied using the molecular-dynamics method. We find that fracture is initiated in an amorphous region at the nanowire surface. Local amorphization propagates across the nanowire while multiple cracks start at the boundaries of the amorphous region. Results for the time evolution of amorphization, crack propagation, and fracture are discussed. [S0031-9007(96)01188-X]

PACS numbers: 61.43.Bn, 61.43.Fs, 62.20.Mk

A great deal of recent research effort has been devoted to understanding the microscopic processes controlling the fracture of materials [1–8]. The key questions in the initiation and development of dynamical fracture relate to conditions for nucleation of cracks, their propagation, and morphology of fracture surfaces. Marder has studied instability in lattice fracture and dynamics of crack propagation [9–11]. First-principles studies of the energies of large scale defects and their implications for brittle-ductile transition have been carried out by Kaxiras and collaborators [12,13]. Recently these issues have been investigated with numerical experiments involving the molecular-dynamics (MD) technique [14,15]. The MD simulations provide detailed information about dislocation emission from crack tips [16], crack branching [17], indentation fracture [18], and brittle-ductile transition [19], etc. Study of amorphization-induced dynamical fracture processes at the atomic level is very promising for understanding problems of enormous technological interest such as size dependence of nanomechanical properties of various one-dimensional nanostructures.

In this Letter, we report the results of MD simulations on amorphization and fracture in silicon diselenide nanowires. $SiSe_2$ has very special crystalline structure. It consists of infinite nonintersecting chains of edge-sharing tetrahedra [20]. Therefore a nanowire containing a finite number of chains can be readily obtained theoretically from a crystalline structure. This material is of great technological usefulness: Silver-doped amorphous $SiSe_2$ is used as a solid electrolyte for advanced high-energy electrochemical cells due to the fast ionic conductivity of Ag in it [21]. The structure and vibrational spectra of crystalline and glassy $SiSe_2$ have been investigated both theoretically and experimentally [22–27]. In amorphous $SiSe_2$ 26% Si atoms occur only in corner-sharing tetrahedra, 22% Si atoms participate exclusively in edge-sharing tetrahedra, and 52% Si atoms are involved in tetrahedra that share one edge [28]. In the MD study of *c*-$SiSe_2$ nanowires containing a finite number (1–64) of chains of edge-sharing tetrahedra, we find that breaking of one bond results in the formation of corner-sharing tetrahedra. This causes local cross-linking of chains and initiates the propagation of local amorphization in the nanowire. Nanowire fractures at the boundaries of the amorphous region after it propagates across the nanowire.

The MD simulations are based on an effective interatomic potential which contains two-body steric repulsion, screened Coulomb interaction due to charge transfer, and a charge-dipole interaction due to large electronic polarizability of selenium ions [21,29–32]. In addition, the effective potential includes the three-body covalent interaction. The MD results for structural correlations and thermodynamic properties are in good agreement with experiments. For example, the calculated melting tempera-

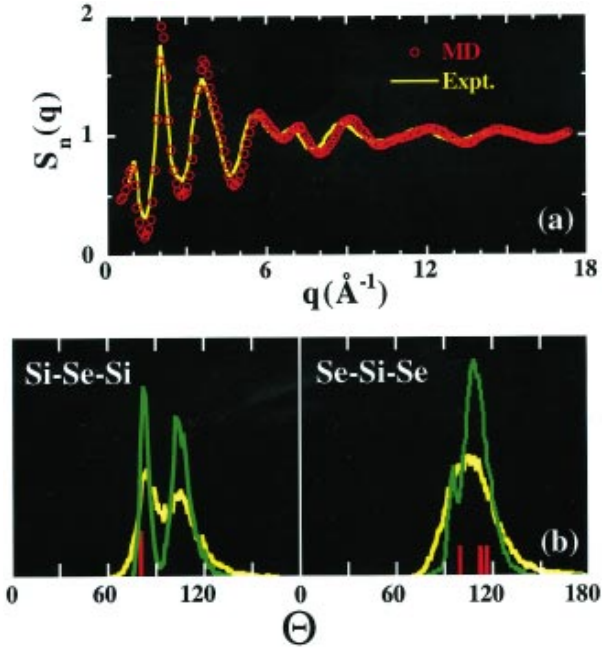

FIG. 1(color). (a) Neutron static structure factor $S_n(q)$ for $SiSe_2$ glass at 200 K. Open circles denote the MD results for a 13 824 particle system, and the solid line shows the neutron diffraction measurements (Ref. [24]); (b) Si-Se-Si and Se-Si-Se bond-angle distributions in crystalline $SiSe_2$ (solid lines with arrow pointed), glassy $SiSe_2$ (dotted lines), and liquid $SiSe_2$ (solid lines).

0031-9007/96/77(11)/2241(4)$10.00

ture $T_m = 1250 + 20$ K compares very well with the experimental value of $1233 + 5$ K [33]. The calculated static structure factor $S_n(q)$ is also in good agreement with the neutron scattering experiment [24]; see Fig. 1(a). Figure 1(b) shows MD results for bond-angle distributions in crystalline, molten, and glassy $SiSe_2$. The second peak in the Si-Se-Si bond-angle distribution around 110° arises from corner-sharing tetrahedra in molten and glassy states.

To prepare $SiSe_2$ nanowires, we first separate a given number (1–64) of adjacent chains from the 3D crystalline configuration. The length of all nanowires is taken to be 3510.6 Å, and their diameters vary from 10 to 60 Å. The number of particles in these nanowires range from 3600 to 230 400. Periodic boundary conditions are applied only along the c axis; nanowires are allowed to move freely along the other two directions. MD simulations are performed with a time step of $\Delta t = 1.45 \times 10^{-15}$ s, which conserves the energy to 1 part in 10^6. Simulations are started from the crystalline configuration of each nanowire. Over a period of 72.5 ps, each nanowire is gradually heated and thermalized at a temperature of 100 K. We then apply a uniaxial strain ε_{zz} to the nanowires. This is done by uniformly scaling the particle coordinates along the c axis. After scaling by 1%, nanowires are thermalized for 4.5 ps. Stable configurations of nanowires are determined by the steepest descent quench scheme [34].

Our MD simulations reveal that all nanowires fracture at the same critical strain ($\varepsilon_{zz} = 15\%$), independent of the number of chains. We keep the strain constant after the critical strain is reached. Figure 2(a) shows a series of snapshots of a 64-chain nanowire projected onto the a-b plane. Here the elapsed time is measured from the moment when critical strain is reached. The number of particles in this nanowire is 230 400. At $t = 6.5$ ps, we observe disordered structure in one of the chains at the outermost layer. As time evolves, the disorder spreads over an increasing number of chains. At $t = 10.9$ ps, all of the chains across the nanowire become disordered. Figure 2(b) shows the same series of snapshots projected onto the b-c plane. In these snapshots, we zoom into the disordered structure (about one-fifth of the whole

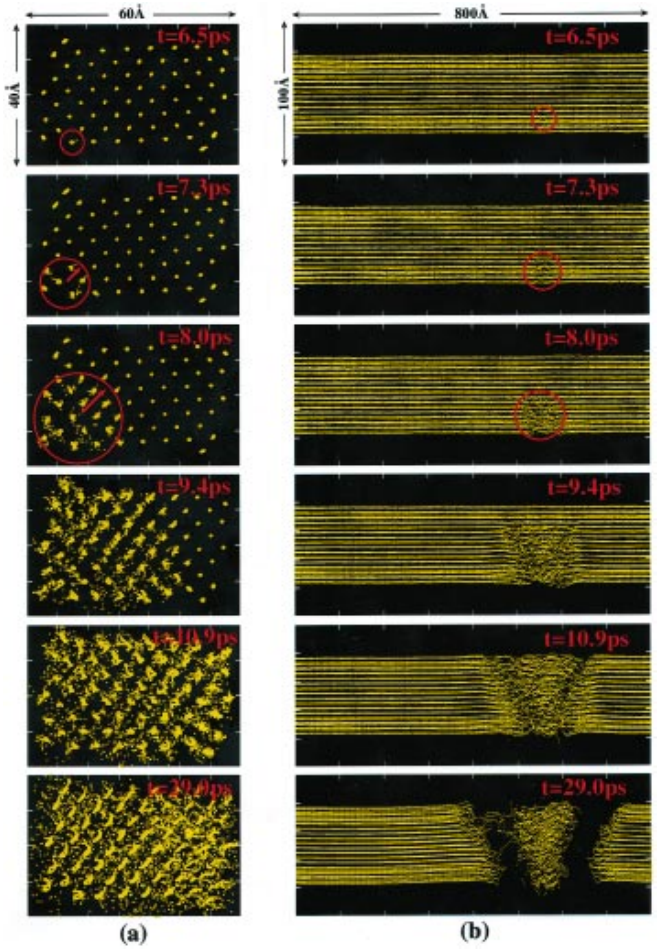

FIG. 2(color). Amorphization and fracture in a 64-chain nanowire. Snapshots of Si atoms projected onto (a) the a-b plane and (b) the b-c plane. Only a segment of the nanowire is presented.

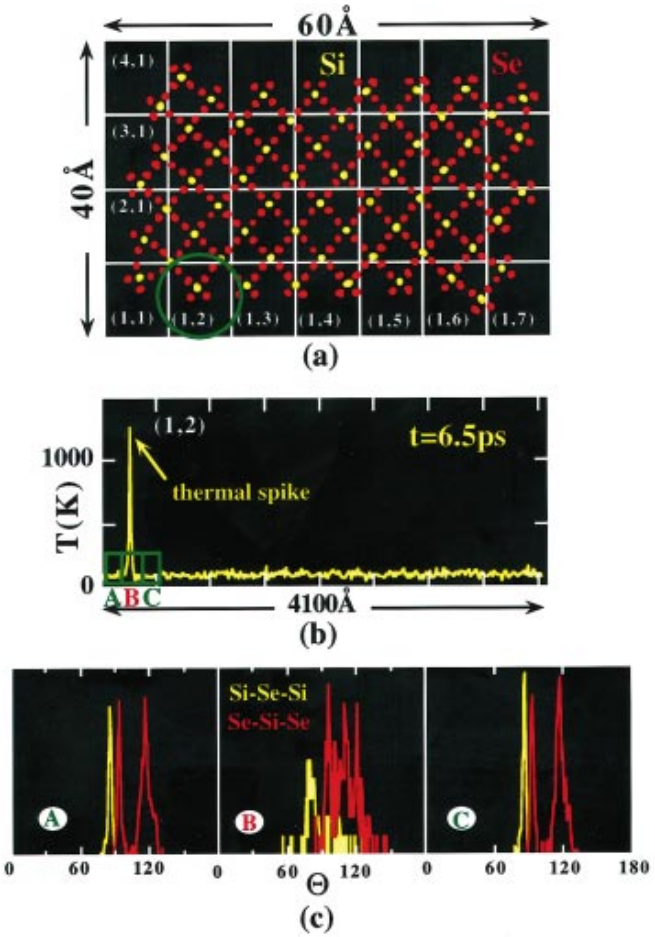

FIG. 3(color). (a) Snapshot of a segment of the 64-chain nanowire projected onto the a-b plane showing Si atoms (yellow) and Se atoms (red). The nanowire is divided into $4 \times 7 \times 300$ cells. (b) Temperature profiles for cells with index (1, 2, $k = 1, \ldots, 300$); (c) local bond-angle distributions for particles in regions A, B, and C.

nanowire). We observe that disorder is localized along the c axis and it expands longitudinally with time. A sandwichlike structure is formed with the disordered region in the middle. At 29.0 ps, the nanowire fractures at one of the two boundaries of this region.

In order to understand the mechanism of dynamical fracture in $SiSe_2$ nanowires, we have investigated the time evolution of temperature and density. The nanowires are divided into cells of dimensions 10 Å $\times$ 10 Å $\times$ 13.5 Å; see Fig. 3(a). There are 4×7 cells on the a-b projection, and we label these cells by their positions on the a-b plane as (i, j) ($i = 1, \ldots, 4$ and $j = 1, \ldots, 7$). Along the c axis there are 300 cells. The cells with indices (1, 2, k; $k = 1, \ldots, 300$) include the site where we first observe the disordered structure. For each cell, we calculate the local temperature. Local bond-angle distributions are analyzed to observe changes in the atomic structure, and the local density is computed to determine where and when a crack starts and how it propagates.

Figure 3(b) shows the "temperature" (here temperature is an estimation of the instantaneous kinetic energy) of the cells with indices (1,2). A thermal spike arises at the site where we first observe the disordered structure. Local-bond angle analysis is then performed for a segment near the thermal spike. This segment is divided into three parts, namely, A, B, and C. Part B includes the cell with the thermal spike, while A and C include several neighboring cells. In Fig. 3(c) we observe large Si-Se-Si angles in part B. They correspond to corner-sharing tetrahedra which arise when edge-sharing bonds are broken in one of the chains at the outermost layer. *Therefore, the disordered structure can be attributed to local amorphization.* The rest of the nanowire remains highly crystalline, as there are well-defined main peaks in bond-angle distributions in parts A and C.

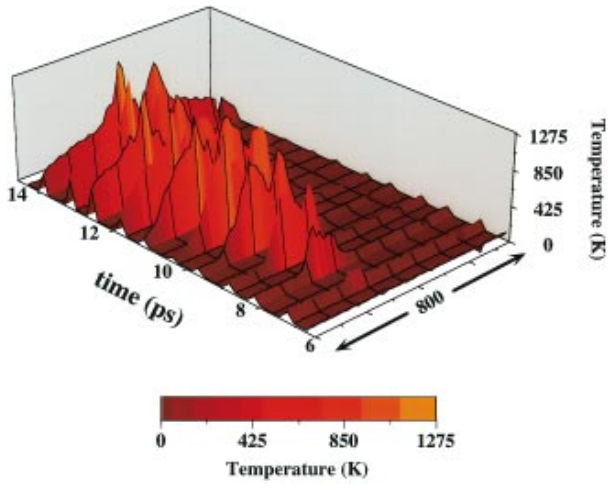

FIG. 4(color). Time evolution of temperature profiles for the 64-chain nanowire. Height and color represent average "temperature" along the nanowire. Only a segment of the nanowire is shown.

Figure 4 shows the time evolution of local temperature. Here the nanowire is sliced into 300 blocks along the c axis, and the temperature is averaged over each block. The x and y axes correspond to the time and the c coordinate along the 64-chain nanowire, respectively. The z axis represents the average local temperature. (Here the temperature is denoted by color; brighter colors correspond to higher temperature.) We have found that the high-temperature region is localized at the fracture site. As time evolves, this region expands along the nanowire while the temperature increases. From the local bond-angle distribution, we find that up to about 10 ps the nanowire in the high-temperature region is in an amorphous state. The rest of the nanowire remains crystalline.

We have examined the local density for each individual cell as well as each block at different time intervals. Figure 5 shows the time evolution of local density. Here the z axis represents the local density averaged over each block. Brighter colors correspond to smaller density. We define a crack when the density of a cell becomes zero. It is observed that up to about 10 ps, there is no crack in the nanowire. At $t = 10$ ps, we observe the nucleation of several cracks. All of the cracks are at the boundaries of the amorphous region, and we clearly observe a drop in the local density at the two boundaries. These cracks propagate inward from the nanowire surface. Local density vanishes at the boundaries when the nanowire completely fractures at about $t = 29$ ps.

In conclusion, these MD simulations reveal that fracture (crack nucleation) in $SiSe_2$ nanowires is preceded by an amorphization process. Amorphization and fracture have also been observed in MD simulations for nanowires with 16 and 32 chains. Thinner nanowires (with the number of chains <16) fail when all of the chains break within a short (<1 ps) time. In order to quantitatively characterize the crack opening mode and the roughness of fracture surface in nanowires, we are performing multi-

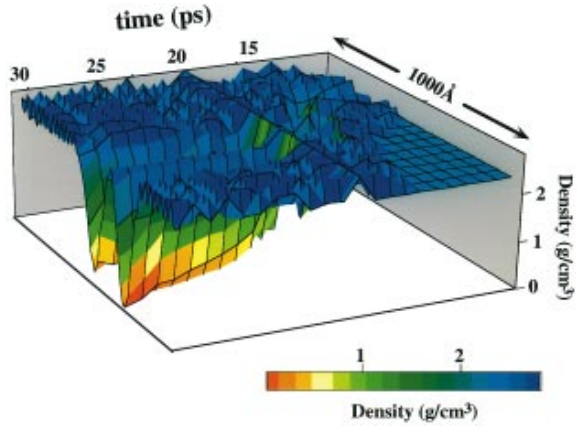

FIG. 5(color). Time evolution of density profiles for the 64-chain nanowire. Height and color represent average density along the nanowire. Only a segment of the nanowire is shown.

million atom MD simulations on parallel architecture for nanowires containing up to 1024 chains. To gain further insight into the microscopics of local amorphization in $SiSe_2$ nanowires and understand the underlying mechanism, we also intend to do the local stress distribution analysis. In addition, the experience of simulating $SiSe_2$ nanowires can be extended to ceramic nanowires such as Si_3N_4 and SiC nanowires. Further results will be presented later.

This work was supported by the U.S. DOE (Grant No. DE-FG05-92ER45477), NSF (Grant No. DMR-9412965), AFOSR (Grant No. F49620-94-1-0444), and USC-LSU Multidisciplinary University Research Initiative (Grant No. F49620-95-1-0452). One of the authors (W. L.) would like to acknowledge the support from NSF Graduate Research Traineeship (Grant No. GER9355007). The simulations are performed on the 40 node Digital Alpha system based on two Gigaswitches in the Concurrent Computing Laboratory for Materials Simulations (CCLMS). The computational facilities in the CCLMS are supported by the Louisiana Education Quality Support Fund (LEQSF).

[1] T. F. Soules and R. F. Busbey, J. Chem. Phys. **78**, 6307 (1983).
[2] J. Kieffer and C. A. Angell, J. Non-Cryst. Solids **106**, 336 (1988).
[3] R. Ochoa *et al.,* J. Non-Cryst. Solids **128**, 57 (1991); R. G. Hoagland *et al.,* J. Mater. Res. **6**, 2565 (1991).
[4] G. J. Dienes and A. Paskin, in *Atomistics of Fracture,* edited by R. M. Latanision and J. R. Pickens (Plenum Press, New York, 1983), p. 671; K. Sieradzki *et al.,* Acta Metall. **36**, 651 (1988).
[5] R. L. B. Selinger *et al.,* Phys. Rev. A **43**, 4396 (1991).
[6] E. Sharon *et al.,* Phys. Rev. Lett. **74**, 5096 (1995).
[7] K. J. Måløy *et al.,* Phys. Rev. Lett. **68**, 213 (1992).
[8] V. Vitek, Mater. Sci. Eng. **94**, 5–69 (1987).
[9] M. Marder, Phys. Rev. Lett. **66**, 2484 (1991).
[10] M. Marder and X. Liu, Phys. Rev. Lett. **71**, 2417 (1993).
[11] M. Marder and S. Gross, J. Mech. Phys. Solids **43**, 1 (1995).
[12] E. Kaxiras and M. S. Duesbery, Phys. Rev. Lett. **70**, 3752 (1993).
[13] Yu-Min Juan *et al.* (to be published).
[14] B. L. Holian and R. Ravelo, Phys. Rev. B **51**, 11 275 (1995).
[15] P. Vashishta, A. Nakano, and R. K. Kalia, in *Proceedings of the 1995 International Conference on Solid State Devices and Materials, Osaka, Japan, 1995* (Publication Office, Business Center for Academic Society Japan, Tokyo, Japan, 1995), pp. 142–144; A. Nakano, R. K. Kalia, and P. Vashishta, Phys. Rev. Lett. **73**, 2336 (1994); **75**, 3138 (1995).
[16] S. J. Zhou and R. Thomson, Phys. Rev. Lett. **72**, 852 (1994).
[17] F. F. Abraham *et al.,* Phys. Rev. Lett. **73**, 272 (1994).
[18] J. Belak *et al.,* Mater. Res. Soc. Bull. **XVIII**, 55 (1993).
[19] K. S. Cheung and S. Yip, Phys. Rev. Lett. **65**, 2804 (1990).
[20] J. Peters and B. Krebs, Acta Crystallogr. B **38**, 1270 (1982).
[21] S. Susman *et al.,* in *Defects in Glasses,* edited by F. L. Galeener *et al.,* MRS Symposia Proceedings No. 61 (Materials Research Society, Pittsburgh, 1986), p. 91.
[22] G. A. Antonio, R. K. Kalia, A. Nakano, and P. Vashishta, Phys. Rev. B **45**, 7455 (1992).
[23] R. Bhadra *et al.,* Phys. Rev. B **39**, 1378 (1989).
[24] R. W. Johnson *et al.,* J. Non-Cryst. Solids **83**, 251 (1986).
[25] L. F. Gladden, J. Non-Cryst. Solids **123**, 22 (1990); S. Sugai, Phys. Rev. B **35**, 1345 (1987).
[26] S. Susman *et al.,* J. Non-Cryst. Solids **106**, 26 (1988).
[27] M. Tenhover *et al.,* Phys. Rev. Lett. **51**, 404 (1983).
[28] M. Tenhover *et al.,* Solid State Commun. **65**, 1517 (1988).
[29] P. Vashishta, R. K. Kalia, J. P. Rino, and I. Ebbsjö, Phys. Rev. B **41**, 12 197 (1990).
[30] W. Jin, R. K. Kalia, P. Vashishta, and J. P. Rino, Phys. Rev. Lett. **71**, 3146 (1993).
[31] A. Nakano, L. Bi, R. K. Kalia, and P. Vashishta, Phys. Rev. B **49**, 9441 (1994).
[32] C. K. Loong, P. Vashishta, R. K. Kalia, and I. Ebbsjö, Europhys. Lett. **31**, 201 (1995).
[33] R. W. Johnson *et al.,* Mater. Res. Bull. **21**, 41 (1986).
[34] F. H. Stillinger and T. A. Weber, Phys. Rev. A **28**, 2408 (1983).